THE ASTROPHYSICAL JOURNAL, 397:520–533, 1992 October 1

IRAS OBSERVATIONS OF YOUNG STELLAR OBJECTS IN THE CORONA AUSTRALIS DARK CLOUD

BRUCE A. WILKING,[1,2,3] THOMAS P. GREENE,[3,4] CHARLES J. LADA,[5]
MICHAEL R. MEYER,[1,3] AND ERICK T. YOUNG[2,3,6]
Received 1992 January 16; accepted 1992 April 8

ABSTRACT

We present an analysis of *IRAS* data for a 57 pc^2 area of the nearby Corona Australis dark cloud complex. A total of 79 far-infrared sources are detected at 12 μm or in at least three *IRAS* bands. Combining these data with both newly obtained and previously published optical/infrared data, a total of 16 *IRAS* sources are identified with young stellar objects which are in close proximity to the R Coronae Australis cloud or Rossano Cloud B. Among these objects is a cold, heavily obscured young stellar object, IRAS 32, which radiates only in the 25–100 μm bands and is found to be associated with an extended near-infrared nebula. The majority of the remaining 63 *IRAS* sources in our sample appear to be related to field stars. A total of 24 young stellar objects are now known to be associated with the Cr A cloud and we investigate their collective properties through analysis of their spectral energy distributions. As observed for embedded populations in other dark clouds, the shapes of the spectral energy distributions constitute a nearly continuous sequence from cold, heavily obscured objects (extreme Class I) to T Tauri stars (Class II), with about equal numbers of Class I and Class II sources. There is a hint of a segregation of the shapes of the spectral energy distributions with source luminosity: eight of nine sources with $L > 1.8\ L_\odot$ display Class I or flat energy distributions. We conclude that star formation in the Cr A cloud has proceeded in a manner similar to that in the ρ Ophiuchi cloud in terms of duration and efficiency. We attribute the relatively low number of young stellar objects in Cr A to its lower mass of both low-density and high-density molecular gas. The luminosity function of the Cr A sources is unique only by the presence of six intermediate-luminosity ($\sim 100\ L_\odot$) objects. Either the cloud has formed intermediate-mass stars more efficiently than lower mass objects relative to other dark clouds or several of these objects are interlopers.

Subject headings: infrared: stars — ISM: clouds — ISM: individual (Corona Australis Cloud)— stars: pre–main sequence

1. INTRODUCTION

Low-mass young stellar objects (YSOs) can display a wide variety of energy distributions as they evolve toward the main sequence. The shapes of these spectral energy distributions (SEDs), determined by the various arrangements of circumstellar dust, are a direct clue to the evolutionary states of the YSOs (e.g., Adams, Lada, & Shu 1987). The majority of the emergent energy from the youngest, most heavily obscured objects is observed at far-infrared wavelengths. On the other hand, the bulk of the luminosity radiated by lightly obscured classical and weak emission T Tauri stars is observed at optical and near-infrared wavelengths. Therefore, a broad range of wavelengths is needed to determine the evolutionary status of a YSO and, by simple integration of its SED, to estimate the YSO's bolometric luminosity. More importantly, confining the study of a YSO population to a narrow wavelength range may bias against the detection of certain classes of YSOs.

There is a growing list of multiwavelength studies of YSO populations in nearby (≤ 200 pc) molecular clouds such as Chamaeleon, Ophiuchus, and Taurus-Auriga (e.g., Prusti, Whittet, & Wesselius 1992; Gauvin & Strom 1992; Wilking, Lada, & Young 1989; Kenyon et al. 1990). YSO populations approaching 100 in number have now been identified in each of these clouds. The cornerstone of these investigations is the data from the *IRAS* survey, particularly the more sensitive co-added survey data and Pointed Observations. These data completely sample the molecular clouds at 12, 25, 60, and 100 μm, with resolution ($\sim 45''$) sufficient to resolve individual YSOs in the shorter wavelength bands. Combining the *IRAS* data with higher resolution ground-based optical and infrared data has several advantages. First, this combination gives the most complete picture of the SED shape and best estimate for the bolometric luminosity of a YSO. Second, we may gain information on lightly obscured YSOs which radiate very little of their luminosity at mid- to far-infrared wavelengths. Finally, we can use the higher resolution data to reduce effectively the source confusion in the *IRAS* data.

The proximity of the Cr A cloud (130 pc, Marraco & Rydgren 1981) makes it an ideal target for multiwavelength studies of its YSO population. Located at $l = 0°$, $b = -18°$, the Cr A dark cloud stretches for about 15 pc in the plane of the sky and is comprised of a centrally condensed molecular cloud on the western edge of the complex (Loren 1979) and two filamentary streamers which extend to the east. The core of the molecular gas in the western complex lies near the emission-line star R Coronae Australis (referred to as the R Cr A cloud)

[1] Department of Physics and Astronomy, University of Missouri-St. Louis, 8001 Natural Bridge Road, St. Louis, MO 63121.
[2] Visiting Astronomer, Cerro Tololo Inter-American Observatory, NOAO, operated by the Association of Universities for Research in Astronomy, Inc., under cooperative agreement with the National Science Foundation.
[3] Visiting Astronomer at the Infrared Telescope Facility, which is operated by the University of Hawaii under contract from the National Aeronautics and Space Administration.
[4] NASA Ames Research Center, MS 245-6, Moffett Field, CA 94035.
[5] Harvard-Smithsonian Center for Astrophysics, MS-72, 60 Garden Street, Cambridge, MA 02138.
[6] Steward Observatory, University of Arizona, Tucson, AZ 85721.

and is a well-studied region of low-mass star formation. It has been the focus of both Hα emission-line surveys (Knacke et al. 1973; Marraco & Rydgren 1981), near-infrared surveys (Vrba, Strom, & Strom 1976a; Taylor & Storey 1984), and far-infrared mapping (Cruz-Gonzales, McBreen, & Fazio 1984; Wilking et al. 1985). Star counts have revealed several cores of enhanced visual extinction in the streamers (Rossano 1978) but these have largely been ignored by near-infrared studies. The most notable of these is Rossano Cloud B which lies about 1°.5 east of the R Cr A cloud core.

We present a study of the YSO population associated with the dark cloud complex in Corona Australis which synthesizes *IRAS* data with newly obtained near- and mid-infrared photometry and previously published optical/infrared data. Our study favors the detection of sources with infrared excesses over lightly obscured pre–main-sequence stars such as weak-emission T Tauri stars. We identify 24 YSOs in the Cr A complex; the observed range of SED shapes and bolometric luminosities are consistent with those observed in other dark clouds. The duration and efficiency of star formation are found to be similar to the ρ Ophiuchi infrared cluster. The low number of YSOs compared to other dark clouds is understood by a reevaluation of the molecular mass of the R Cr A cloud which shows it to be much less massive than previously assumed. A possible variation in the mass function of YSOs relative to the ρ Oph cloud is briefly discussed.

2. OBSERVATIONAL PROCEDURE AND EQUIPMENT

2.1. *IRAS Data*

2.1.1. *Intensity Map at 100 μm*

An image of the *IRAS* 100 μm intensity map is shown in orthographic projection in Figure 1 (Plates 6 and 7). The image is the result of mosaicing two adjacent fields produced using the BIGMAP utility which coadds the survey scans, destripes the field, and maps the 3′ × 5′ resolution data into 1′ pixels. In order to show most clearly the low-level emission from the cloud filaments, a linear gray scale has been used such that emission from the warm, high column density core is saturated. In the absence of heat sources, the 100 μm intensity has been shown to be a good tracer of column density in dark clouds, with values for $I_\nu(100\ \mu m)/A_v$ ranging from 5 to 8 MJy sr^{-1} mag^{-1} (see Boulanger 1989 for review). Hence the lowest contours of I_ν in Figure 1 of 7.2, 10.0, 12.8, 15.7, and 18.5 MJy sr^{-1} correspond roughly to $A_v = 1.1$, 1.5, 2.0, 2.4, and 2.8 mag, respectively. These values are in good agreement with those in the 15′ resolution extinction map determined from star counts (Rossano 1978).

2.1.2. *Analysis of Point and Small Extended Sources*

We have considered an 11.1 deg^2 (57 pc^2) area of the Corona Australis dark cloud complex from $\alpha(1950) = 18^h52^m$ to 19^h20^m and $\delta(1950) = -36°30'$ to $-38°30'$. This area, shown in Figure 1, was selected on the basis of the *IRAS* 100 μm intensity map and star counts to encompass the high-density core region as well as most of the filamentary streamers where visual extinctions are greater than 1.0 mag. Three types of *IRAS* data were analyzed in this region. Co-added survey data, 3 times more sensitive at 12 μm than the *IRAS* Point Source Catalog (1985, hereafter, PSC) in regions of low source density, were analyzed for a 7 deg^2 area including the highest extinction regions of the cloud. The PSC was examined for the unconfused, outer fringes of the cloud ($\delta = -38°$ to $-38°.5$). Both of these data sets have a full width at half-power (FWHP) angular resolution at 12 and 25 μm of about 0′.76 in the in-scan direction (roughly north-south in declination) and 3′.5 in the cross-scan direction. High-resolution Pointed Observations of the high source density cloud core were analyzed in 12 overlapping fields, covering a 0.25 deg^2 area. The FWHP angular resolution for each field at 12, 25, 60, and 100 μm is about 0′.76 × 1′.18, 0′.76 × 2′.33, 1′.51 × 1′.28, and 3′.03 × 2′.52, respectively. For analysis, these fields were mapped onto a grid of 30″ pixels. These data allowed us to measure flux densities for two sources (TS 13.1 and VSS 10) confused in the co-added survey data.

Except for the two sources mentioned above, all flux densities were determined from one-dimensional in-scan profiles obtained from the ADDSCAN data product using the weighted mean of all survey passes. No color corrections have been made. Photometric calibration was based upon the same absolute calibration as the PSC. Over most of the region of interest, photometric uncertainties are estimated to be ±15% but may be as large as ±50% in the high source density core. In-scan source sizes (FWHP) given in Tables 1 and 2 were determined by deconvolving the source with a gaussian beam characteristic of a point source.

Positions, flux densities, and source widths for 79 *IRAS* sources extracted from the three data sets are presented in Tables 1 and 2. Upper limits to the flux densities are quoted as 3 times the rms noise; typical values in regions of low source density were 0.04, 0.06, 0.10, and 1.0 Jy for the four *IRAS* bands. Flux densities followed by a colon are 3–5 times the rms noise and are considered uncertain. Table 1 lists 15 objects which display $S_\nu(25\ \mu m)/S_\nu(12\ \mu m) > 0.8$ and Table 2 lists 64 objects with ratios less than 0.8. A ratio of 0.8 corresponds to a spectral index $a = -1.33$, where a is defined as $d \log (\lambda S_\lambda)/d \log \lambda$. Such a spectral index is characteristic of an infrared excess produced by an optically thick, spatially thin disk with a $r^{-0.75}$ temperature gradient (see § 3). Sources with steeper slopes are most likely field stars. For inclusion in these tables, sources were required either to be detected at 12 μm or in at least three *IRAS* bands. These criteria excluded most cirrus-type sources except for IRAS 18577−3707 in Table 1 and *IRAS* 18535−3718 in Table 2 which are associated with late-type B stars and radiate in all four *IRAS* bands. Most of the sources (61 of 79) listed in Tables 1 and 2 are found in the PSC. However, using the improved signal-to-noise provided by the co-added survey data, we were able to detect known sources in the longer wavelength bands, determine integrated flux densities and source sizes for extended sources, and separate sources confused in the PSC.

2.2. *Near–Infrared Observations*

Images at J (1.25 μm), H (1.65 μm), K (2.2 μm), and L (3.5 μm) were obtained for 23 *IRAS* sources in the vicinity of the high extinction core, excluding sources with well-observed near-infrared counterparts. Infrared array cameras were used with the 1.5 m telescope at Cerro Tololo Inter-American Observatory (CTIO) and the 3.0 m Infrared Telescope Facility in Hawaii (IRTF). Near-infrared sources were detected in close proximity to the *IRAS* source positions in all cases but one (IRAS 14). The positions and fluxes in magnitudes for the 54 sources found in the course of these observations are presented in Table 3. The magnitudes presented are in their respective photometric systems: the CIT/CTIO system (Elias et al. 1983) and the ProtoCAM/IRTF system (Ressler & Shure 1992, private communication). The observing and reduction procedures for these two sets of observations are described below.

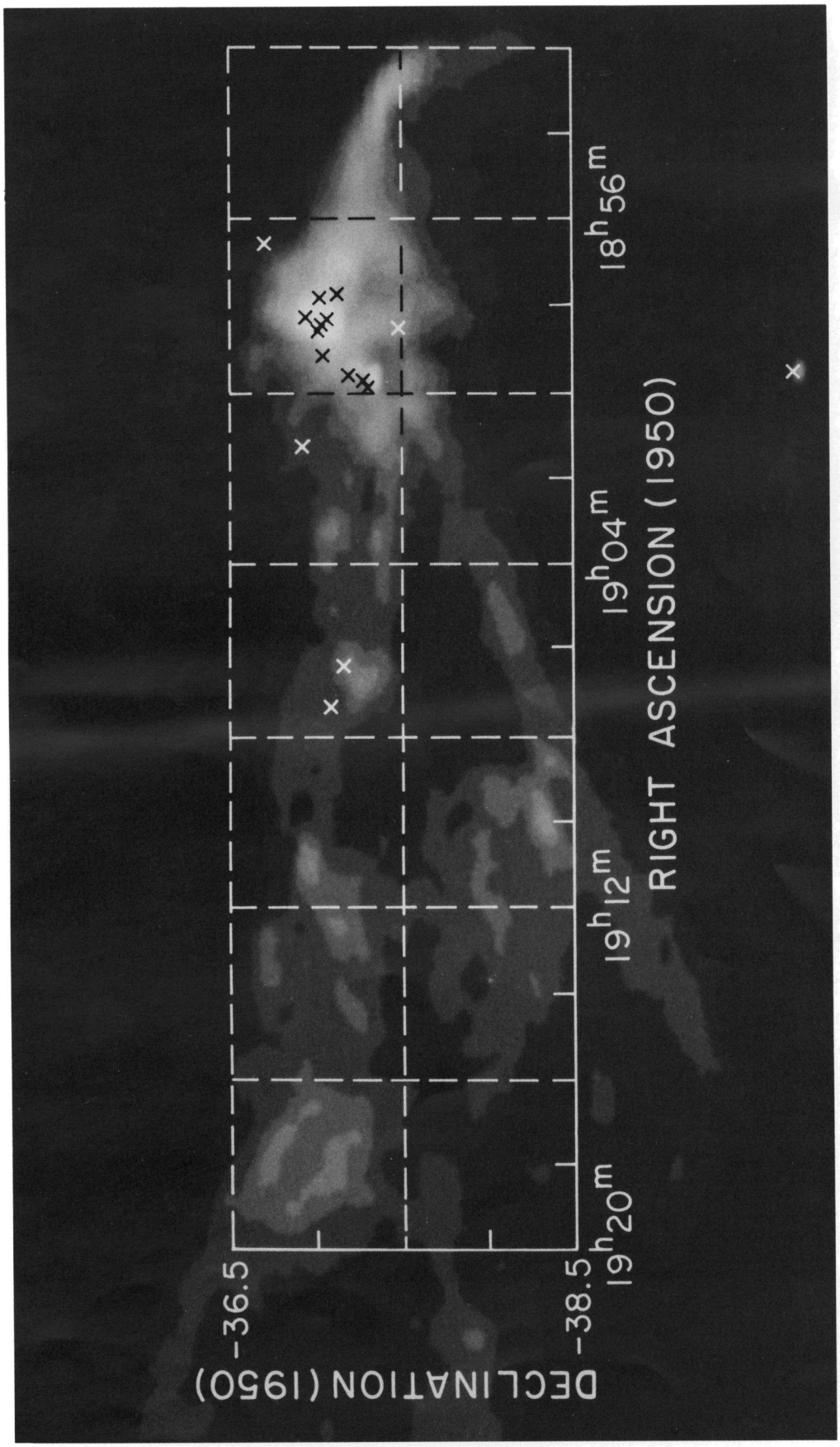

FIG. 1*a*

FIG. 1.—Linear gray-scale image of the *IRAS* 100 μm intensity which defines the boundaries of the Corona Australis dark cloud. The gray levels begin at 7.2 MJy sr^{-1} and increase in units of 2.8 MJy sr^{-1}. Fig. 1*a* shows the distribution of the 15 *IRAS* sources with $S_\nu(25\ \mu m)/S_\nu(12\ \mu m) > 0.8$ relative to the dark cloud, and Fig. 1*b* shows the distribution of the 64 *IRAS* sources with $S_\nu(25\ \mu m)/S_\nu(12\ \mu m) < 0.8$.

PLATE 7

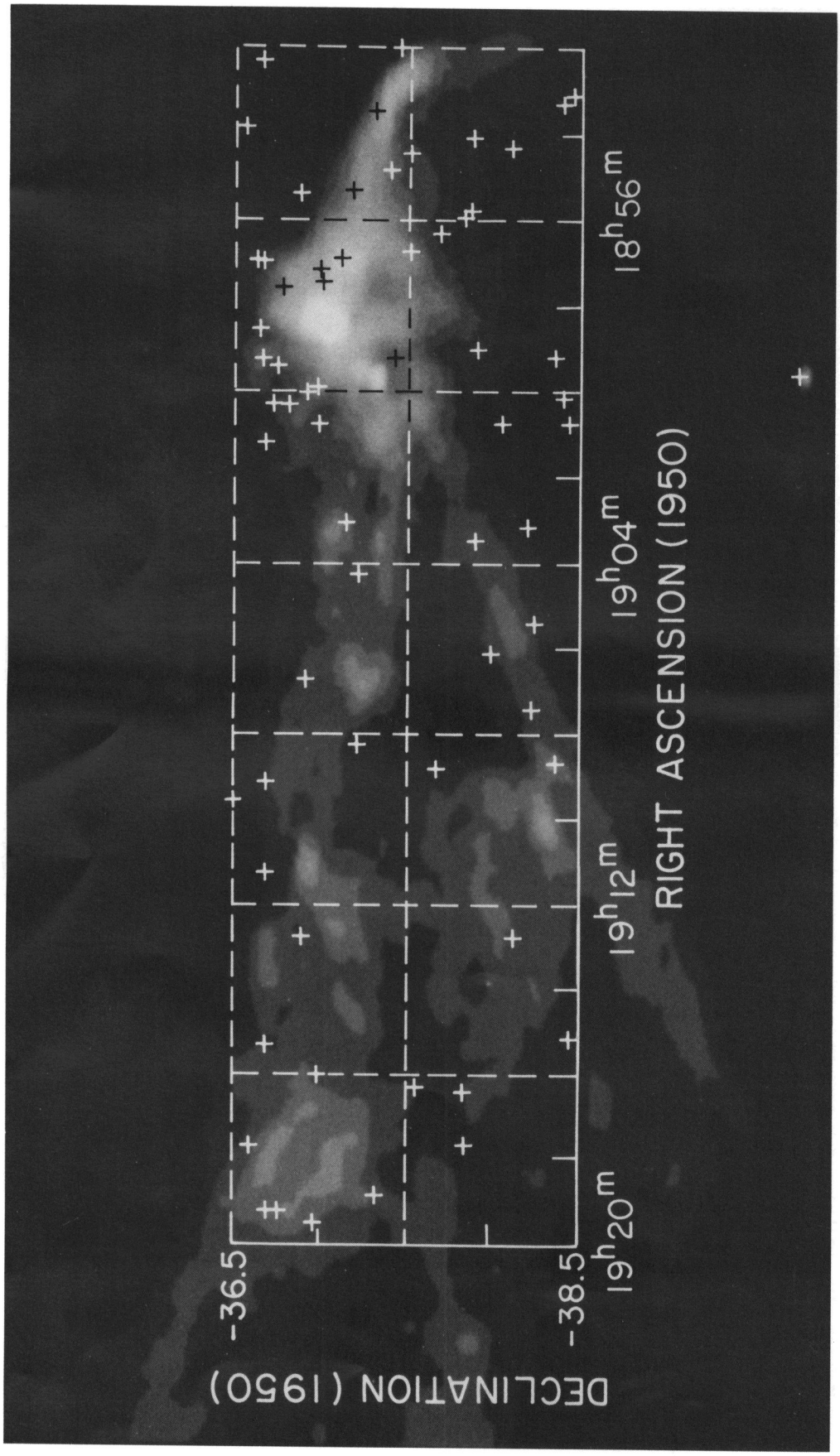

FIG. 1*b*

WILKING et al. (see 397, 521)

TABLE 1

IRAS SOURCES WITH $S_\nu(25\ \mu m)/S_\nu(12\ \mu m) > 0.8$: R.A. (1950) = 18^h52^m TO 19^h20^m, Decl. (1950) = $-36°30'$ TO $-38°30'$

Source No. (1)	R.A. (1950) (2)	Decl. (1950) (3)	$S_\nu(12)$ (Jy)(a) (4)	W(12) (')(b) (5)	$S_\nu(25)$ (Jy) (6)	W(25) (') (7)	$S_\nu(60)$ (Jy) (8)	W(60) (') (9)	$S_\nu(100)$ (Jy) (10)	W(100) (') (11)	Visible Star?(c) (12)	Associations/ Notes (d) (13)
10	$18^h56^m38.6^s$	-36°41'25"	0.18	0.35	0.24	0.68	<0.50	-	<3	-	TT/yes	Hα6,Hα5,iras10a+b,(1)
18	18 57 41.5	-37 07 59	1.1	0.59	2.0	0.91	4.7	2.6	c	-	B8V/B8V	SAO210815+6,(2)(3)
19	18 57 47.0	-37 01 36	4.9	PS	9.5	PS	19	PS	28	PS:	TT	S CrA,(1)(4)
20	18 58 17.2	-36 57 02	63	0.86	110	0.78	660	1.3	1400	2.6	B8V/A0V	TY CrA,HD176386,(2)(5)
21	18 58 18.9	-37 02 50	13:	PS	50:	PS	85:	PS	c	-	no	TS13.1,(5)(6)
23	18 58 28.2	-37 02 29	15	PS	53	PS	140	PS	c	-	no	HH100-IR,(5)(7)
24	18 58 30.7	-37 28 05	0.87	PS	2.0	PS	3.2	PS	2.5:	PS	TT	DG CrA
25	18 58 32.9	-37 01 27	125	PS	270	PS	610	PS	1160	PS	A5p/no	R CrA,R1,R2,(5)(6)(7)
28	18 59 07.4	-37 02 44	0.59	PS	0.49	PS	0.55:	PS	c	-	TT/yes	Hα14,Hα3,(1)
32	18 59 35.8	-37 11 53	<0.13	-	3.8	PS	38	PS	55	PS	no	iras32c,d,e,(1)
33	18 59 43.9	-37 17 16	33	PS	69	PS	130	PS	100	PS	TT	VV CrA,(1)(8)
34	18 59 53.1	-37 18 33	0.55:	PS	1.6:	PS	1.9:	-	c	-	no	VSS10,(1)(9)
	19 01 17.5	-36 55 31	0.50:	1.5:	0.40:	0.7:	1.1	1.6	1.5:	PS:	B9.5V	SAO210888,(1)
	19 06 23.8	-37 09 18	0.55	PS	1.5	PS	2.4	0.66	9.5	3.0	yes	Hα16,(1)(10)
	19 07 21.5	-37 04 11	0.38	PS	0.64	0.55	0.54	1.9	<3.3	-	yes	Hα17,(1)(10)

[a] Flux densities and source sizes followed by a colon are uncertain due to low signal-to-noise and/or source confusion. "c" indicates source confusion which did not permit a flux determination. All flux densities were determined from in-scan slices using the ADDSCAN utility, except for Sources 21 and 34 which were derived from the Pointed Observations.

[b] Source size is given in arcminutes, deconvolved with a Gaussian beam of 0.'76 (12 μm), 0.'77 (25 μm), 1.'39 (60 μm), or 2.'96 (100 μm). "PS" denotes where source size is consistent with point source.

[c] "TT" denotes T Tauri star. References to spectral types and Hα emission from Knacke et al. 1973 and Marraco & Rydgren 1981.

[d] Notes on individual sources: (1) Near-infrared photometry for 2 μm sources presented in Table 3. (2) Extended emission associated with visible reflection nebula. (3) Source is badly confused in all bands. Integrated fluxes are greater than 60 Jy at 60 μm and greater than 240 Jy at 100 μm. (4) S Cr A is a double with separation of 1.'4 (Herbig 1962). (5) Far-infrared source also mapped by Cruz-Gonzales, McBreen, & Fazio 1984 and/or Wilking et al. 1985. (6) TS 13.1, R1, and R2 are from the 2 μm survey of Taylor & Storey 1984. (7) The HH 100-IR source is confused with R Cr A. Flux densities for both sources were derived assuming R Cr A is a point source in all bands. (8) VV Cr A is a double star with separation of 2" with companion brightest in the infrared (B. Reipurth 1991, private communication). (9) VSS 10 is from the 2 μm survey of Vrba, Strom, & Strom 1976a. (10) Source associated with Cloud B (Rossano 1978).

2.2.1. *CTIO Observations*

J, *H*, *K*, and *L* band data were obtained with the CTIO InSb array imager during the period 1989 July 12–19. The effective plate scale was 0.''89 pixel^{-1} resulting in a field of view in α and δ of 55" × 52". Observations were made in a beam-switching mode with the *IRAS* source position centered in the eastern half of the array in the first frame followed by a sky frame offset 33" east. The sky frame often contained a second, independent image of the primary source. This mode allowed a coverage of a 88" × 52" area, with the long dimension nearly parallel to the *IRAS* cross-scan direction for this region. Maps of several sources (IRAS 12, 16, 26, and 32) were made covering a 107" × 104" area by stepping the array in 26" steps. The limiting magnitudes (5 σ) for the CTIO observations at *H*, *K*, and *L* were roughly 14, 15, and 7.5 mag in 60, 60, and 30 seconds of integration. Infrared standards from the list of Elias et al. (1982) and the star A0 V star HD 176386 (Taylor & Storey 1984; Wilking, Taylor, & Storey 1986) were observed frequently throughout the night and were used to estimate the extinction per air mass at *H* and *K*, typically 0.10 and 0.05 mag per air mass, respectively. An unreddened 2 μm source, HD 176386b, was found 3.''8 from the standard star HD 176386; they are clearly resolved in apertures of 6" or less.

The data were reduced using standard routines within the Image Reduction and Analysis Facility (IRAF) supplemented by custom scripts and C language programs. Processing of data frames consisted of first removing a master bias frame determined for each night and then applying a linearization correction to the data. The linearized data were used in all subsequent steps of the reduction. Bad pixels were determined for each day at each wavelength and removed from the data frames through interpolation. Flat fields were constructed for each filter by median filtering several dark-subtracted data frames of mostly blank sky. Each data frame was subtracted by a corresponding sky frame to remove thermal backgrounds and other systematic offsets. These sky-subtracted frames were then divided by the flat fields which were normalized by their mean pixel values. Photometry was then performed using the APPHOT package in IRAF through apertures of diameter 3", 4", and 6" with a sky annulus centered on the source with an

TABLE 2 FOOTNOTES

[a] Flux densities followed by a colon are uncertain due to low signal-to-noise or source confusion. "c" indicates where source confusion did not permit a flux determination. All flux densities were determined using ADDSCAN. Upper limits are 3 times the rms noise. Except where noted in col. (9), all in-scan source sizes are consistent with point sources.

[b] "Yes" denotes star(s) of magnitude 13 or brighter at photographic *B* or *V* within 45" in r.a. and 25" in decl. of the *IRAS* position. Star names are from either the SAO catalog or the Guide Star Catalog. Spectral classifications are given as recorded in the SIMBAD database.

[c] Notes on individual sources: (1) Also GSC 7421.0894. (2) Cirrus heated by nearby B8 IV star (Leene 1986). Deconvolved source sizes are $W(12) = 1.'9$, $W(25) = 3.'0$, $W(60) = 1.'8$, and $W(100) = 4.'1$. See Leene for integrated fluxes. (3) Mira variable (Feast 1963). (4) A foreground eclipsing binary star (Tapia & Whelan 1975). (5) Photometry for 2 μm sources associated with *IRAS* source is presented in Table 3. (6) Visible star in polarimetric study by Vrba, Strom, & Strom 1976b (VSSb) or Vrba, Coyne, & Tapia 1984 (VCT). (7) Deconvolved source sizes are $W(12) = 0.'82$, $W(25) = 1.'1$, and $W(60) = 1.'0$. (8) *IRAS* LRS spectrum displays 10 μm emission feature plus "blue" continuum characteristic of an AGB star (Olnon & Raimond 1986). (9) Also GSC 7917.0901 which appears to be variable. (10) A foreground star which is double (Penny 1979). (11) A foreground star, HR 7232. (12) A foreground star, HR 7254.

TABLE 2

IRAS SOURCES WITH $S_\nu(25\ \mu m)/S_\nu(12\ \mu m) < 0.8$: R.A. (1950) = 18^h52^m TO 19^h20^m, Decl. (1950) = $-36°30'$ TO $-38°30'$

Source No. (1)	R.A. (1950) (2)	Decl. (1950) (3)	$S_\nu(12)$ (Jy)(a) (4)	$S_\nu(25)$ (Jy) (5)	$S_\nu(60)$ (Jy) (6)	$S_\nu(100)$ (Jy) (7)	Visible Star?(b) (8)	Associations/ Notes (c) (9)
	$18^h52^m00.3^s$	-37°27′05″	1.1	0.31:	<0.92	<7.2	K1III	SAO210716
	18 52 21.6	-36 38 38	0.30	<0.11	<0.14	<0.68	K3III	SAO210723,(1)
	18 53 07.1	-38 28 31	0.64	0.22	<0.14	<0.88	yes	GSC7916.2092,.0717
	18 53 17.9	-38 23 22	0.44	<0.12	<0.24	<0.51	yes	GSC7916.1359
	18 53 29.5	-37 18 12	1.4	0.53	6.0	47	no	cirrus,(2)
	18 53 52.1	-36 32 43	3.9	1.8	0.40	<0.74	yes	GSC7421.1228
	18 54 07.0	-37 52 01	7.5	4.3	0.61	<1.0	M6e	UX CrA, (3)
	18 54 21.6	-38 06 21	0.45	<0.26	<0.18	<0.40	yes	GSC7916.0280
	18 54 27.4	-37 31 01	1.1	0.54	<0.15	<2.6	yes	GSC7421.0005
1	18 54 51.7	-37 23 07	2.5	0.70	0.20	<5.8	K5/M0III	SAO210766
3	18 55 19.7	-37 10 34	1.4	0.33:	<0.60	<1.0	F2V	ϵ CrA,SAO210781,(4)
4	18 55 25.6	-36 52 42	0.49	<0.25	<0.25	<1.2	yes	iras4a,b,(5)
5	18 55 47.9	-37 50 55	0.64	<0.15	<0.25	<2.0	no	
7	18 55 57.9	-37 49 10	0.39	0.22:	<0.30	<0.60	yes	GSC7916.0457
8	18 56 19.1	-37 40 31	0.38	0.25	<0.20	<1.8	yes	GSC7916.0149
11	18 56 45.9	-37 30 27	0.35	<0.22	<0.50	<6.0	yes	iras11,(5)
12	18 56 54.0	-37 06 19	0.20:	<0.25	<1.6	<9.0	no	iras12a,b,g,(5)
13	18 56 58.6	-36 36 54	0.23	<0.11	<0.15	<2.0	yes	iras13a,b,(5)
14	18 56 59.4	-36 39 02	0.25	<0.20	<0.20	<2.0	no	
15	18 57 11.3	-36 59 15	0.22:	<0.20	<1.1	c	no	iras15,(5)
16	18 57 26.4	-37 00 09	0.35:	<0.20	<0.44	c	no	iras16a,b,c,d,(5)
17	18 57 35.3	-36 46 05	3.6	1.5	<0.50	<4.7	M5III	VSSb28,iras17b,(5)(6)
26	18 58 32.2	-36 37 46	0.53	<0.15	<0.20	<1.1	yes	iras26a,b,c,d,(5)
27	18 59 01.7	-37 54 10	0.77	0.25	<0.25	<1.6	K5	SAO210846
29	18 59 12.7	-37 25 37	0.30	<0.10	<0.23	<14	yes	iras29a,b,(5)
	18 59 13.2	-38 21 29	3.8	0.91	0.18	<1.0	M2/M3III	SAO210851
30	18 59 16.5	-36 40 17	0.15:	<0.25	<0.30	<1.1	yes	GSC7421.1662
31	18 59 22.6	-36 43 57	3.0	0.90	<0.40	<5.2	M1III	SAO210854,(5)
35	18 59 55.0	-36 58 01	0.52	<0.20	<0.20	<2.8	K5III	VSSb22,(5)(6)
36	19 00 00.2	-36 55 44	0.20:	<0.15	<0.30	<2.4	K1III	VCT84,(5)(6)
	19 00 11.1	-38 24 49	5.4	2.4	0.50	<0.70	yes	VX CrA,(7)
37	19 00 16.0	-36 49 40	0.38	<0.20	<0.20	<1.0	no	iras37a,b,(5)
38	19 00 19.3	-36 43 09	0.42	<0.20	<0.15	<3.6	yes	iras38,(5)
	19 00 45.6	-38 02 53	0.55	<0.12	<0.13	<0.90	yes	GSC7917.0106
	19 00 45.9	-38 26 38	260	180	31	11	yes	RAFGL5553,(8)(9)
39	19 00 49.5	-36 58 48	0.14:	<0.12	<0.12	<3.6	G6/G8III	SAO210875
40	19 01 17.1	-36 40 05	0.15:	<0.10	<0.10	<1.0	yes	GSC7422.0240
	19 03 02.1	-37 08 25	3.0	0.65	<0.33	<6.9	F7IV-V	γ CrA,SAO210928,(10)
	19 03 08.8	-38 12 17	1.0	0.38	<0.16	<0.60	M0III	SAO210931
	19 03 29.6	-37 53 14	0.64	0.26	<0.23	<2.0	G5IV	SAO210937,(11)
	19 04 15.9	-37 13 06	0.30	0.23	<0.15	<5.3	no	
	19 05 25.7	-38 14 54	0.75	0.18	<0.19	<2.9	K3III	SAO210978
	19 06 04.5	-37 59 08	1.2	0.32	<0.14	<3.7	A2V	α CrA,SAO210990,(12)
	19 06 41.1	-36 54 43	0.33	0.22	<0.13	<1.3	G8IV	SAO211007
	19 07 24.8	-38 13 25	0.42	<0.16	<0.60	<2.0	yes	GSC7918.1356
	19 08 13.1	-37 12 28	0.77	0.19	<0.15	<1.2	no	
	19 08 40.4	-38 22 09	0.97	0.20	<0.27	<7.1	yes	GSC7918.1462
	19 08 48.8	-37 40 00	1.1	0.24	<0.12	<2.2	G2III	SAO211037
	19 09 07.0	-36 40 09	1.3	0.46	<0.25	<3.6	K5	SAO211040
	19 09 35.6	-36 30 38	0.67	0.20	<0.15	<2.0	yes	GSC7435.0883
	19 11 17.6	-36 39 42	0.49	<0.13	<0.11	<0.70	K3/K4III	SAO211078
	19 12 44.0	-36 53 32	0.76	0.20	<0.10	<5.7	yes	GSC7435.0183
	19 12 46.5	-38 08 05	0.24	<0.12	<0.12	<3.4	yes	GSC7918.0213
	19 15 10.3	-38 28 01	0.70	<0.19	<0.26	<1.4	K5/M0III	SAO211151
	19 15 17.1	-36 40 18	52	32	5.7	1.8	Me	V924 Sgr,(8)
	19 16 01.3	-36 59 14	0.84	0.21	<0.19	<2.0	K1III/IV	SAO211166
	19 16 17.3	-37 31 55	19	12	1.8	1.3	yes	GSC7435.0621,(8)
	19 16 26.5	-37 49 47	0.57	<0.19	<0.22	<4.7	yes	GSC7918.0138
	19 17 40.7	-37 50 49	0.42	<0.12	<0.15	<0.40	yes	GSC7931.0327
	19 17 41.1	-36 34 16	1.1	0.27	0.15	<4.6	yes	GSC7436.1420
	19 18 49.9	-37 18 58	0.37	<0.11	<0.21	<2.2	G8III	SAO211212
	19 19 10.0	-36 41 05	1.1	0.33	<0.13	<1.9	no	
	19 19 13.2	-36 45 24	0.54	<0.19	<0.13	<1.6	no	
	19 19 29.0	-36 57 43	0.30	<0.15	<0.11	<0.60	no	

TABLE 3

NEAR-INFRARED PHOTOMETRY OF *IRAS* SOURCES

Name	R.A. (1950)	Decl. (1950)	Vis? (a)	Flux in Magnitudes (b) J	H	σ	K	σ	L	Obs.	Notes (c)
(1)	(2)	(3)	(4)	(5)	(6)	(7)	(8)	(9)	(10)	(11)	(12)
iras4a	$18^h55^m24.9^s$	-36°52′43″	yes		5.62		5.40		5.08	CTIO	GCS,(V=11.79)
iras4b	18 55 27.7	-36 53 03	no		8.70		8.86	0.09	>6.7	CTIO	
iras10a	18 56 37.2	-36 41 36	yes		8.19		8.14			CTIO	GSC,(V=10.95)
				8.70	8.29		8.20		8.15	IRTF	σ(L)=0.05
iras10b	18 56 37.8	-36 41 19	yes		11.49		11.32	0.09	>7.5	CTIO	
				12.01	11.55		11.40	0.10		IRTF	σ(J)=0.17
Hα6	18 56 39.5	-36 41 19	TT	10.78	9.85		9.35		8.69	IRTF	σ(L)=0.10
Hα5	18 56 40.0	-36 41 54	yes	13.20	12.76		12.30	0.20		IRTF	
iras10c	18 56 41.9	-36 41 25	yes	11.54	11.29		11.19		10.5:	IRTF	
iras11a	18 56 44.4	-37 30 30	yes				5.23		4.92	CTIO	GSC,(V=10.39)
iras12e	18 56 50.4	-37 06 45	no		14.50	0.10	13.99	0.16		CTIO	
iras12a	18 56 51.3	-37 05 57	no		13.06		12.56		>7.5	CTIO	K(4″)
iras12g	18 56 52.1	-37 06 41	no		15.04	0.08	14.51	0.13		CTIO	HK(4″)
iras12h	18 56 54.5	-37 07 06	no		15.37	0.18	>14.4			CTIO	H(4″)
iras12c	18 56 54.9	-37 06 48	no		14.20		13.80	0.14		CTIO	(d)
iras12d	18 56 55.6	-37 07 02	no		14.62	0.11	14.15	0.15		CTIO	HK(4″)
iras12f	18 56 56.0	-37 06 48	no		15.14	0.15	14.47	0.19		CTIO	HK(4″),(d)
iras12b	18 56 56.8	-37 06 37	no		13.27		12.89		>7.5	CTIO	
iras13a	18 56 57.7	-36 37 02	yes		8.52		8.33		7.91	CTIO	GSC,(V=12.41)
iras13b	18 57 00.3	-36 36 54	no		12.88	0.08	12.93	0.21		CTIO	HK(4″)
iras15a	18 57 14.4	-36 59 14	no		6.97		6.14			CTIO	
iras16a	18 57 22.7	-37 00 15	no		14.10	0.11	13.35	0.07	>7.5	CTIO	
iras16d	18 57 24.1	-37 00 05	no		>15.0		14.58	0.20		CTIO	K(4″)
iras16c	18 57 26.8	-37 00 07	no				13.91	0.15		CTIO	
iras16b	18 57 28.3	-37 00 33	no		14.99	0.15	13.62		>7.5	CTIO	HK(4″)
iras17b	18 57 36.1	-36 46 19	no				7.82	0.18	>7.5	CTIO	
iras17a	18 57 36.7	-36 46 01	K5III		3.68		3.37		3.23	CTIO	VSSb28,(e)
S Cr A	18 57 46.0	-37 01 37	yes	8.11	7.06		6.29	0.05		IRTF	double
HD176386b	18 58 16.8	-36 57 47	?		9.10		8.88	0.06	8.75	CTIO	HKL(3″),(f)
iras26a	18 58 27.4	-36 37 47	yes		5.38		5.19			CTIO	GSC,(V=10.50)
iras26b	18 58 31.0	-36 37 52	no		13.39		13.49	0.18		CTIO	
iras26c	18 58 35.7	-36 38 00	no		14.49	0.12	14.45	0.25		CTIO	HK(4″)
iras26d	$18^h58^m35.8^s$	-36°37′31″	no		14.64	0.13	14.59	0.24		CTIO	HK(4″)
Hα 14	18 59 04.3	-37 02 38	TT		8.21		7.96		7.40	CTIO	H(4″),GPl2,(g)
				8.98	8.14		7.83			IRTF	
Hα 3	18 59 10.6	-37 02 46	yes		8.98		8.51	0.10	7.55	CTIO	GPz
iras29b	18 59 13.2	-37 25 46	no		10.30	0.12	9.91		>7.5	CTIO	
iras29a	18 59 14.4	-37 25 34	yes		6.43		6.26		5.90	CTIO	GSC,(V=10.65)
iras31a	18 59 22.2	-36 43 50	M1III		3.29		3.05			CTIO	SAO210854,(V=8.18)
iras31b	18 59 26.7	-36 43 46	no		7.68		7.52	0.07		CTIO	
iras32c	18 59 35.9	-37 12 00	no		>15.7		13.52	0.07	>7.5	CTIO	extended
					16.30	0.20	13.80	0.10		IRTF	HK(8″)
iras32b	18 59 36.7	-37 11 17	no	>16.4	15.63	0.17	13.31	0.08		CTIO	
iras32e	18 59 38.3	-37 11 56	no		>15.0		14.79	0.32	>7.5	CTIO	
iras32d	18 59 38.5	-37 12 12	no		>15.7		13.78	0.10	>7.5	CTIO	
iras32a	18 59 40.1	-37 11 30	no	15.70	12.74		11.14		>7.5	CTIO	σ(J)=0.10
				15.59	12.63		11.20			IRTF	
VV Cr A	18 59 43.7	-37 17 15	TT				4.55			CTIO	(f)
				8.61	6.77		5.11		3.26	IRTF	
VSS10	18 59 53.5	-37 18 32	no		9.98		8.92		7.52	CTIO	
iras35a	18 59 55.9	-36 57 56	K3III		5.40		5.01		4.66	CTIO	VSSb22,(e)
iras36a	19 00 02.4	-36 55 37	K1III		6.45		6.18		6.07	CTIO	VCT84,(e)
iras37b	19 00 13.2	-36 49 17	no		12.83		13.00	0.07	>7.5	CTIO	
iras38a	19 00 17.8	-36 43 08	yes		5.65		5.49		5.19	CTIO	GSC,(V=10.57)
iras37a	19 00 19.0	-36 49 56	no		12.65		12.50		>7.5	CTIO	
iras37c	19 00 20.2	-36 50 02	no		14.53	0.19			>7.5	CTIO	
SAO210888	19 01 22.2	-36 55 12	yes	7.73	7.62		7.60		7.63	IRTF	
Hα16	19 06 23.7	-37 09 18	yes	9.68	8.71		8.41			IRTF	
Hα17	19 07 21.3	-37 04 06	yes	10.17	9.37		9.07	0.09		IRTF	

[a] "Yes" denotes either star was visible in focal plane camera ($V < 14$ mag) or has published spectrum as referenced in col. (12). "TT" denotes a T Tauri star.

[b] Magnitudes at H and K are given in cols. (6) and (8) and are followed by their statistical one sigma errors in cols. (7) and (9), respectively, when they exceed absolute uncertainties. L photometry is quoted for a 4″ (CTIO) or 6″ aperture (IRTF). H and K photometry are quoted for a 6″ aperture, except where noted in col. (12).

[c] Source names from Glass & Penston 1975 (GP), Vrba, Strom, & Strom 1976a (VSS), Vrba, Strom, & Strom 1976b (VSSb), Marraco & Rydgren 1981 (Hα), Vrba, Coyne, & Tapia 1984 (VCT), and the Guide Star Catalog (GSC, Lasker et al. 1990).

[d] Magnitudes could be slightly underestimated due to faint source in sky annulus.

[e] Spectral type from Vrba & Rydgren 1984.

[f] Companion to HD 176386. Magnitudes could be slightly overestimated due to contamination from primary.

[g] Spectral type from Marraco & Rydgren 1981.

inner radius of 6″ and an outer radius of 12″. The infrared standards mentioned above were used to calibrate the fluxes, and apply atmospheric extinction corrections whenever possible. Atmospheric corrections were not possible at *L*, however these effects were minimized by calibrating the images to standards observed closely in time and at a similar air mass. Uncertainties in this process, as well as random errors due to the detector and sky noise, are reflected in standard deviations quoted for the photometry.

The photometry are presented in Table 3. Magnitudes at *H* and *K* are quoted for a 6″ aperture in most cases, while sky noise limitations required the use of a 4″ aperture at *L*. Uncertainties in the absolute calibration were estimated by comparison of our data with that obtained with the IRTF (see next section) and by Vrba & Rydgren (1984); these errors are believed to be ± 0.06 mag for *J*, *H*, and *K*. Uncertainties at *L* are ± 0.15 mag for bright sources but larger for fainter objects due to difficulties in flat-fielding the data. Errors for the photometry are quoted when they exceed these values. Source positions in Table 3 were determined relative to a reference area on the array whose position was fixed by offsets from nearby SAO stars. Absolute uncertainties in these positions are better than 5″, reflecting errors in pointing and tracking.

2.2.2. *IRTF Observations*

Additional *J*, *H*, *K*, and *L* band photometry were obtained at the IRTF in 1990 June and 1991 May with the ProtoCAM imager equipped with an InSb array. These data are also presented in Table 3. The effective plate scale for the observations was 0.″35 pixel^{-1} resulting in a field of view in α and δ of 22″ × 20″. Observations were made in a beam-switching mode with an offset 8″ south. All photometry were calibrated relative to observations of HD 176386 closely spaced in time, minimizing errors due to sky variations and differences in air mass. Absolute uncertainties in the photometry are estimated to be ± 0.04.

Magnitudes and positions were determined in a manner similar to that described for the CTIO data with the following variations. For the data from 1990, variations in our short duration (0.2 s) zero bias exposures prevented us from constructing flat fields from that data set. Instead, we constructed flat fields at *J*, *H*, *K*, and *L* using 1990 October ProtoCAM data which had slightly longer (1 s) zero bias exposures that did not exhibit excessive variations. These flat fields were made by median filtering many high signal-to-noise dark-subtracted exposures of mostly blank sky in each band. Photometry was performed through an aperture of 6″ with a sky annulus centered on the source with an inner radius of 5″ and an outer radius of 10″.

For the 1991 data set, flat fields at *J*, *H*, and *K* were constructed by differencing an image of an illuminated dome target with that of an unilluminated image, thus subtracting thermal emissions plus any electronic offsets. At *L*, where thermal emission from the dome and telescope are much greater, a flat was constructed by differencing an image of a dome target with that of blank sky. Photometry was then performed using apertures of diameter 6″ with a sky annulus centered on the source with an inner radius of 5″ and an outer radius of 7″.

2.3. *Mid-Infrared Observations*

Sources confused or extended in the *IRAS* 12 μm data were targeted for mid-infrared observations. Photometry at *M* (4.8 μm), *N* (10.2 μm), and *Q* (20 μm) were obtained with the IRTF bolometer on 1991 May 21–22 using an aperture of 3 mm (5.″5). *M* photometry for Hα6 was obtained on 1990 June 26 using a 4 mm (7.″5) aperture. These data are presented in Table 4. Absolute calibration was established relative to the primary standard γ Aql and the secondary standard ν^2 Sgr.

3. RESULTS

3.1. *The Distribution of IRAS Sources*

A clue to the nature of the *IRAS* sources can be deduced from their distribution relative to the dark cloud material. Figure 1*a* shows the distribution of *IRAS* sources from Table 1 with $S_\nu(25\ \mu m)/S_\nu(12\ \mu m) > 0.8$. These sources are confined to the vicinity of the two densest molecular clumps: the R CrA cloud (Rossano Cloud A) and Rossano Cloud B. In contrast, the distribution of *IRAS* sources with $S_\nu(25\ \mu m)/S_\nu(12\ \mu m) < 0.8$, presented in Figure 1*b*, is much more uniform across the complex. While there is a somewhat higher density of these sources toward the R Cr A cloud, they avoid the highest column density regions. Utilizing the grid of 0.8 deg^2 boxes in Figure 1*b*, we can discuss this distribution more quantitatively. The average number of sources per box outside of the R Cr A cloud core and Rossano Cloud B is about 3.6 (4.5 sources deg^{-2}). Only the area comprising the R Cr A cloud core has a significantly higher density of sources with S_ν(25

TABLE 4

MID-INFRARED PHOTOMETRY OF *IRAS* SOURCES

Source	Flux in Magnitudes (a)					Notes
	M	σ	N	σ	Q	
(1)	(2)	(3)	(4)	(5)	(6)	(7)
iras10a	8.18	0.15	>6.2	...	...	
Hα6	8.1	0.3	...	...	...	
Hα14	7.16	0.15	5.57	0.13	...	
Hα3	6.84	...	5.42	0.13	...	
VV Cr A	1.98	...	0.03	...	-1.91	(b)
SAO210888	7.93	0.18	>6.2	...	...	
Hα16	...	...	4.73	...	...	
Hα17	7.60	0.14	5.14	...	...	

[a] We estimate the uncertainty in the absolute calibration of the photometry to be about 10%. The magnitudes at *M* and *N* in cols. (2) and (4) are followed by their statistical one sigma errors in cols. (3) and (5), respectively, when they exceed 10%. All observations were made through a 5.″5 aperture except for Hα6 where a 7.″5 aperture was used. Upper limits are 3 times the rms noise.

[b] Peak flux measured toward infrared companion.

μm)/S_ν(12 μm) < 0.8 than this background level; assuming Poisson noise, the 11 sources in this area are nearly 4 standard deviations from the average across the cloud. Therefore, the picture revealed by considering the distribution of *IRAS* sources relative to the cloud is that most of the sources from Table 1 are intimately associated with the molecular gas. In contrast, the more uniform distribution of sources from Table 2 is consistent with the idea that these objects represent the background population of *IRAS* sources at this Galactic latitude, with the possible exception of sources on the periphery of the R Cr A cloud.

3.2. *The Nature of the IRAS Sources*

Several strategies were used to identify the optical/near-infrared counterparts to the *IRAS* sources in our study. These counterparts were required to lie within 45″ of the *IRAS* position in α and 25″ in δ. First, the SIMBAD data base was searched for associations with SAO stars, variable stars, or previously observed infrared sources. Published spectral types are listed in the column preceding these associations when available. Particular attention was paid to Hα emission line stars observed by Knacke et al. (1973) and Maracco & Rydgren (1981), and infrared sources reported by Vrba et al. (1976a, b, hereafter VSS, VSSb) and Taylor & Storey (1984, and unpublished observations, hereafter TS). Further associations with visible stars were obtained from the Guide Star Catalog (Lasker et al. 1990, hereafter GSC); only GSC stars with photographic *B* or *V* magnitudes of 13 or brighter are noted in Table 2. Identifications for three *IRAS* sources were aided by mid-infrared spectra obtained by the Low Resolution Spectrometer (Olnon & Raimond 1986). Finally, near-infrared counterparts for 22 *IRAS* sources were identified through the imaging described in § 2.2.

Optical/near-infrared counterparts were identified for most of the *IRAS* sources and are listed in columns (13) and (9) of Tables 1 and 2, respectively. The character of these counterparts confirms the nature of the *IRAS* sources inferred from their distribution relative to the dark cloud. All of the 15 *IRAS* sources with S_ν(25 μm)/S_ν(12 μm) > 0.8 (Table 1) have counterparts which are young stars or YSOs associated with the Cr A cloud. They include six early-type stars (producing four *IRAS* sources), seven emission-line stars, and four embedded YSOs. The evolutionary status of these objects is discussed further in the following section. In contrast, many of the 64 *IRAS* sources with S_ν(25 μm)/S_ν(12 μm) < 0.8 (Table 2) are associated with field stars. Four of these *IRAS* sources are identified with foreground stars, while 20 coincide with late *G*, *K*, or *M* giants. In addition, the SEDs for seven *IRAS* sources with near-infrared counterparts but no published spectral types are indistinguishable from those of the background *G*, *K*, and *M* giants (see § 3.3) and are also likely to be background objects. Consequently, many of the *IRAS* flux densities in Table 2 should be color corrected which would reduce the 12 and 25 μm flux densities by 40% and the 60 μm flux density by 30%.

While the natures of the remaining 33 *IRAS* sources in Table 2 are uncertain, most have optical counterparts in the *GSC* and, away from the R Cr A cloud, their distribution is indistinguishable from that of the known field stars. Therefore it is likely the majority are late-type field stars; optical spectra and/or near-infrared photometry are needed to determine precisely their nature. Possible exceptions include IRAS 13, which has an apparent infrared excess at 3.4 and 12 μm, and the cirrus source/B8 IV star IRAS 18535−3718 (Leene 1986). As discussed in the previous section, the enhanced density of *IRAS* sources toward the periphery of the R Cr A cloud suggests that several could be association members; on the other hand, our failure to construct reasonable SEDs for four *IRAS* sources in this area (§ 3.3) suggests that some could be 12 μm cirrus illuminated by nearby late *B* stars.

3.3. *Spectral Energy Distributions*

We can use the energy distribution of an *IRAS* source over the 1–100 μm spectral range to make inferences about its evolutionary state (e.g., for review see Adams et al. 1987; Lada 1988; Wilking et al. 1989). Each SED is characterized by its spectral index, *a*, computed from 2.2 μm to the longest wavelength observed among 10, 12, 20, or 25 μm. A value of $a = 0$ corresponds to a flat-spectrum source. SEDs with $a > 0.2$ are categorized as Class I and arise from heavily obscured YSOs; sources in this class have been modeled successfully as accreting protostars (Adams et al. 1987). Flat-spectrum sources display $0.2 > a > -0.2$ and represent YSOs believed to have either active or flared disks (e.g., Adams et al. 1988). SEDs with $-2 < a < -0.2$ are defined as Class II and are usually found toward visible YSOs in a T Tauri-phase of evolution. Class III SEDs exhibit an $a < -2$ and have little or no infrared excess. These SEDs usually peak at far-visual/near-infrared wavelengths and are found associated with weak-emission T Tauri stars or field stars. Finally, double-peaked SEDs are classified as either Class IID or IIID, depending on whether the wavelength of the first peak is in the near-infrared or visual. The former SEDs are believed to arise from heavily obscured YSOs with stellar winds which have begun to dissipate their outer dust envelopes while the latter are associated with early-type stars which heat extended nebulae of cool dust.

There are a total of 36 objects in Cr A for which SEDs could be constructed and spectral indices determined. These data are summarized in Table 5. Twenty-four sources in this sample display either Class I, II, IIID, or flat SEDs and comprise the known population of young stars in this cloud. In addition to the *IRAS* sources presented in this study, we have included seven sources with previously published ground-based mid-infrared photometry which are confused in the *IRAS* data: data for R1, R2, TS 2.4, T Cr A, TS 2.8, HD 176386, and TS 3.5 were taken from the study by Wilking et al. (1986). In cases where several optical/near-infrared counterparts were associated with an *IRAS* source, it was usually clear from their near-infrared colors which source dominates in the far-infrared. However, in three cases the relative contributions of several near-infrared sources to the *IRAS* flux density could not be disentangled and these are presented as single sources IRAS 32c and d, VV Cr A and its infrared companion (B. Reipurth 1991, private communication), and SAO 210815/210816. Spectral indices are not presented for IRAS 14 (no counterpart) nor for IRAS 12, 16, and 37 (the near-infrared SED does not join smoothly with the *IRAS* data). In the latter group, either the true near-infrared counterparts have yet to be discovered or the *IRAS* sources are due to externally heated dust.

The distribution of spectral indices is shown in Figure 2. Considering the small number of objects, the distribution is relatively flat and continuous for Class I and II objects. This is consistent with the idea that Class I YSOs evolve into Class II objects (Adams et al. 1987). There are roughly equal numbers of Class I and Class II objects in our sample. Seven sources are classified as Class I objects ($2.3 > a > 0.2$), four have flat SEDs ($0.2 > a > -0.2$), and eight objects are Class II objects

TABLE 5

SPECTRAL INDICES AND LUMINOSITIES

Source	Spectral a	Index $2.2\text{-}\lambda_f(\mu m)$	Luminosity ($L_\odot$) L(fir)	L'(obs)	$\lambda_i\text{-}\lambda_f$ (μm)	L''(obs)
(1)	(2)	(3)	(4)	(5)	(6)	(7)
SAO210815	-1.2 (IIID)	-	0.31	42	0.44-100	280(a)
SAO210816						
TY Cr A	0.80 (IIID)	-	40	33	0.36-100	140(b)
R Cr A	0.19	25	50	78	0.36-100	96
SAO210888	-1.2 (IIID)	-	0.11	5.3	0.44-100	90(c)
HD176386	-1.6 (IIID?)	10	-	13	0.36-10	80(d)
VV Cr A	0.0	25	10	22	0.36-100	24
HH100IR	1.0	25	7.1	11	1.25-60	14
TS13.1	0.67	25	5.5	9.5	1.25-60	12
S Cr A	-0.37	25	1.6	5.1	0.36-100	5.5
R1	2.3	20	-	2.3	1.25-20	5.2
T Cr A	0.89	20	-	1.6	0.36-20	3.4
TS2.4	1.3	20	-	2.1	1.25-100	3.0
IRAS32	2.0	25	1.6	2.5	2.20-100	2.4(e)
R2	1.8	20	-	0.54	1.25-20	1.0
Hα16	-0.32	25	0.27	0.86	0.44-100	1.0
DG Cr A	-0.14	25	0.28	0.68	0.36-100	0.72
IRAS13	-1.2	12	0.03	0.69	0.44-12	0.72
Hα14	-1.3	25	0.05	0.66	0.44-60	0.67(f)
VSS10	-0.10	25	0.17	0.38	1.65-60	0.43
Hα3	-1.0	25	0.05	0.38	0.44-60	0.39(f)
Hα17	-0.43	25	0.08	0.26	1.25-60	0.28
Hα6	-0.71	25	0.03	0.21	0.44-25	0.22
TS2.8	-0.35	10	-	0.05	1.25-10	0.07
IRS10a	<-1.7	10				
IRAS29	-2.1	12				
IRAS17	-2.2	25				
IRAS4	-2.3	12				
IRAS38	-2.4	12				
SAO210851	-2.4	25				
IRAS15	-2.4	12				
IRAS26	-2.4	12				
IRAS36	-2.4	12				
TS3.5	-2.5	10				
IRAS35	-2.5	12				
IRAS31	-2.6	25				
IRAS11	-2.6	12				

[a] Combined luminosity for two B8 V stars.
[b] Luminosity for B8 V star.
[c] Luminosity for B9.5 V star.
[d] Luminosity for A0 V star.
[e] Extended near-infrared radiation not included in final luminosity estimate.
[f] 50% of 12–60 μm flux density from IRAS 28 attributed to source.

($-0.2 > a > -1.3$). There is a marked peak in the distribution of Class III sources at $a = -2.4$. Five of these 10 sources have published spectral types classifying them as K/M giants, and by implication the remaining five *IRAS* sources, as well as IRAS 29 ($a = -2.1$) and IRAS 11 ($a = -2.6$), are also probably background stars. As alluded to earlier, we have not applied color corrections to the *IRAS* data but note here that for Class III sources, the effect would be to decrease a spectral index of -2.4 (2.2–25 μm) to -2.5.

The spectral energy distributions plotted in Figures 3*a*–3*c* for 25 *IRAS* sources were produced by combining our data with data from the literature. No attempt has been made to adjust the flux densities of a source for the fact that observations have been made with different beam sizes or the fact that sources are often variable over time. Not shown in Figure 3 are SEDs for sources confused in the *IRAS* data; these SEDs have already been presented in Wilking et al. (1986). Also not shown are the Class IIID SEDs observed for the 5 B8–A0 spectral type stars; the extended nature of their dust emission renders their *IRAS* flux densities more uncertain. The range of spectral shapes in Figure 3 are similar to those observed in other dark clouds. Sources with Class I or flat SEDs are presented in Figure 3*a*. In this group, IRAS 32 is an example of an extreme Class I source. It has no pointlike component at wavelengths shorter than 25 μm but is associated with a heavily reddened, extended patch of nebulosity observed at *H* and *K*. IRAS 32 joins a growing list of extremely cold objects found in molecular cloud cores which includes IRAS 16293−2422 and B335 (e.g., Lada 1991). SEDs are presented in Figure 3*b* for Class II objects. All of these objects are visible stars which appear to be in a T Tauri phase of evolution. Hα6 and S Cr A are classified as T Tauri stars and another four objects have been reported to display Hα emission (Marraco & Rydgren 1981). Sources with Class III SEDs are presented in Figure 3*c*. The SEDs for the K

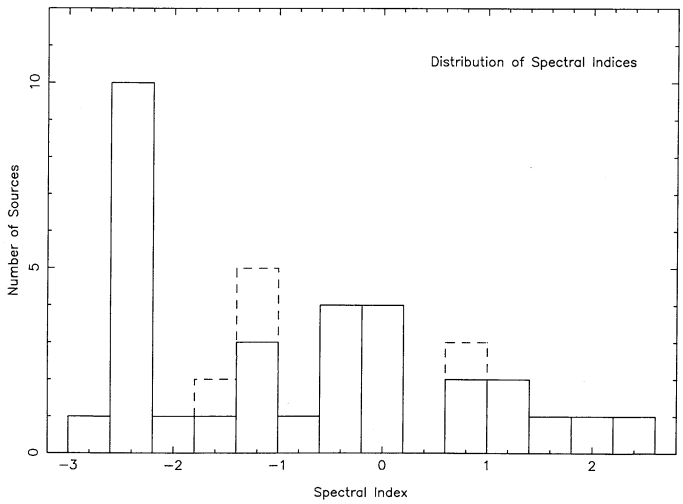

FIG. 2.—Distribution of spectral indices for 36 sources. Included in the sample are the 4 Class IIID sources listed in Table 5 (*dashed lines*) and IRAS 10a for which only an upper limit to spectral index is known.

and M giants IRAS 17, 31, 35, 36, and SAO 210851 are indistinguishable from the remaining Class III objects which have not been observed spectroscopically.

3.4. *Luminosity Function*

An estimate for the bolometric luminosity of a YSO can be obtained by simple integration of its spectral energy distribution. In most cases, these estimates are believed to be within a factor of 2 of the true luminosity; we refer the reader to Wilking et al. (1989) for a detailed discussion of the uncertainties of this technique. Briefly, the major uncertainties arise from the assumptions that the luminosity is radiated isotropically and that foreground extinction by dust can be ignored. These assumptions are most valid for Class I objects which are likely obscured by a spherical circumstellar envelope which absorbs and reradiates most of the energy from the central source (e.g., Adams et al. 1987). For Class II and flat-spectrum sources, a large fraction (25%–40%) of the luminosity may be radiated by a circumstellar disk; the assumption of isotropic radiation can lead to *overestimates* for the bolometric luminosity by as much as a factor of 2 depending on the inclination angle. Our inability to deredden these sources can result in an *underestimate* of their luminosity by about a factor of 2. The bolometric luminosities for Class IIID sources in our sample were not determined from their SEDs but rather from their spectral types, assuming they lie on the main sequence.

Luminosities estimated for the 24 Class I and Class II YSOs in this region are presented in Table 5. In column (4), the 7–135 μm luminosity [L(fir)] has been computed by summing the in-band fluxes in the four *IRAS* broad-band filters (Emerson 1988). The next column presents the observed luminosity, L'(obs), obtained by integrating the SED over the observed range of wavelengths (listed in col. [6]). Finally in column (7), the observed luminosity extrapolated to infinite wavelength L''(obs), is presented (except for Class IIID sources as noted above). The nature of the extrapolation is arbitrary and we have chosen to assume a spectral index of $a = -1$ from the longest wavelength observed. A comparison of columns (5) and (7) shows that the observed luminosities for sources confused in the *IRAS* data are uncertain by about a factor of 2 due to the lack of data beyond 20 μm. The luminosity function of these sources is shown in Figure 4, using the luminosities from column (7).

There is a hint of luminosity segregation among Class I and II YSOs similar to that observed in the ρ Oph cloud. For example, of the nine YSOs with $L > 1.8\ L_\odot$, eight are either Class I or flat-spectrum sources with the double star S Cr A having the only negative spectral index (-0.37). In contrast, of the nine sources with $0.18\ L_\odot < L''(\text{obs}) < 1.8\ L_\odot$, only three are either Class I (R2) or flat-spectrum (DG Cr A, VSS10) sources. However, the number of sources involved is much less than that observed in ρ Oph and it will be important for future space and ground-based infrared studies of the lower luminosity sources to confirm this effect.

4. COMPARISONS WITH THE ρ OPHIUCHI CLOUD

To understand more clearly the nature of star formation in the Cr A cloud, it is instructive to compare the properties of its embedded population with that of a similar cloud. The ρ Ophiuchi cloud is quite similar to Cr A in terms of its distance (160 vs. 130 pc) and angular extent (10–15 pc). The molecular gas is distributed in a large, centrally condensed core and two filamentary streamers. The numbers of intermediate-luminosity stars ($L > 18\ L_\odot$) in ρ Oph is the same as found in Cr A (seven). Both clouds are devoid of any massive stars (B0 V or earlier).

The ages of these star-forming regions also appear comparable. An age of $1.5–3.5 \times 10^6$ yr is estimated for the ρ Oph core (Wilking et al. 1989). This is based partially on the contraction time for the least massive star on the main sequence, the B9–A0 star SR-3 (Lada & Wilking 1984). In the Cr A cloud, the B8 star TY Cr A and the A0 star HD 176386 appear to be near if not on the main sequence. Neither star has optical line emission nor large near-infrared excesses at 2.2 μm (Marraco & Rydgren 1981; Wilking et al. 1986). Based on the double-peaked SED for TY Cr A and theoretical models by Yorke (1980), Cruz-Gonzales et al. (1984) estimate an age of about 1.5×10^6 yr for the star which is close to its contraction age (e.g., Iben 1965). In contrast, the star R Cr A which has been measured to have a spectral type of A5 is clearly above the main sequence. Estimates for the star's luminosity range from 96 $L_\odot$ (this study) to 148 $L_\odot$ (Cruz-Gonzales et al. 1984) and are in excess of the main-sequence luminosity for an A star. Hence, we estimate the age of the cloud to lie between the contraction ages of a B8 and A5 star: $1.5–5.9 \times 10^6$ yr.

Despite the many similarities between the ρ Oph and Cr A clouds, there are striking differences in the relative numbers and distributions of luminosities of their YSOs which we describe below.

4.1. *Fewer Young Stellar Objects in Corona Australis*

The number of *IRAS* sources associated with the Cr A cloud (16) is much less than the number observed in ρ Oph (44, Wilking et al. 1989). As a result, the number of YSOs with reliable bolometric luminosity estimates in Cr A (24) is less than half that in ρ Oph (58). One might suspect that the fewer number of *IRAS* sources in Cr A could be due to selection effects arising from high visual extinctions in the core or confusion in the *IRAS* data. But observations support neither of these explanations. We have made $C^{18}O$ ($J = 1–0$) observations of the R Cr A core and derived gas column densities and visual extinctions using the same techniques employed for the ρ Oph core (Wilking & Lada 1983). Compared to the ρ Oph core, the main R Cr A core is smaller (0.024 vs. 0.55 pc^2, where

1992ApJ...397..520W

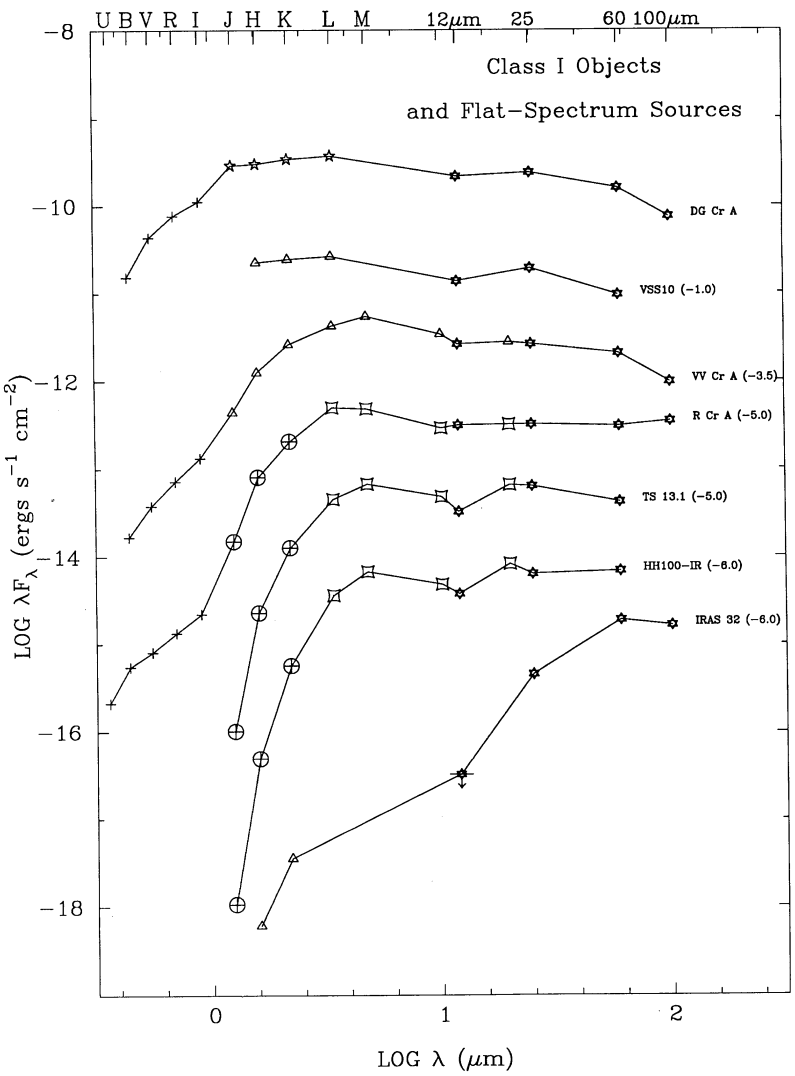

FIG. 3*a*

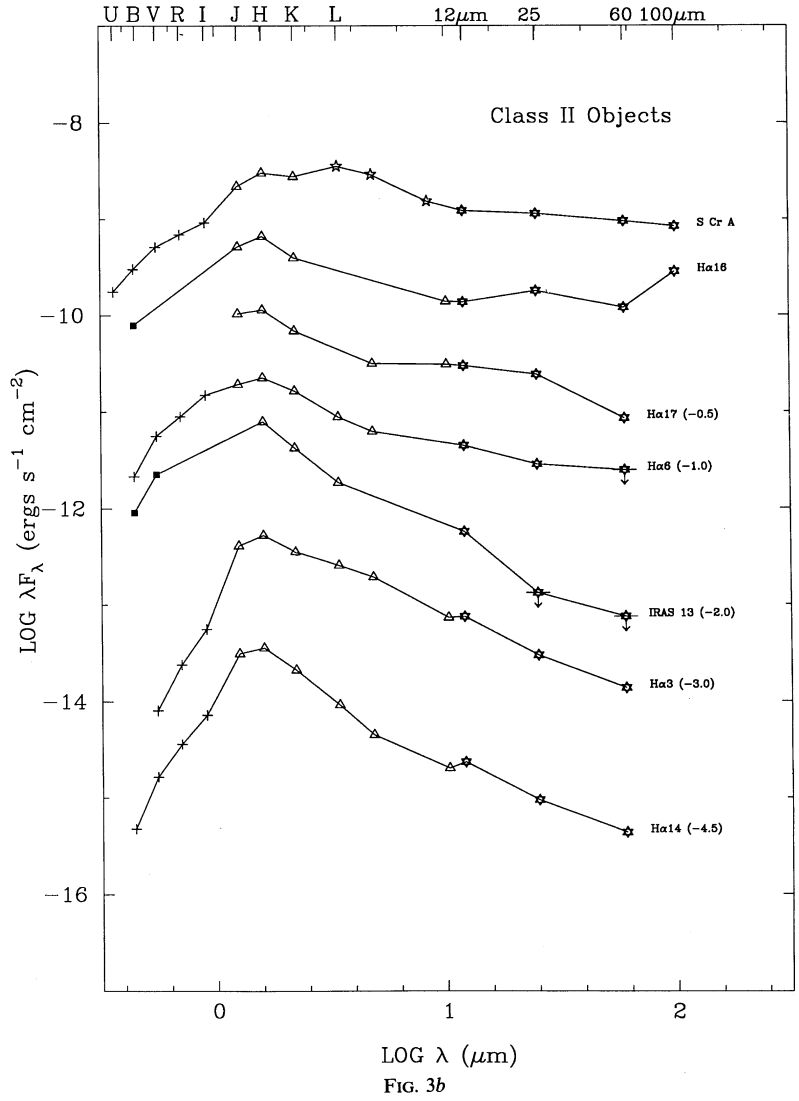

FIG. 3*b*

FIG. 3.—Spectral energy distributions for selected *IRAS* sources in Cr A. Sources with previously published SEDs or Class IIID SEDs are not included. To the right of the source name is the power of 10 used to scale the SED. *IRAS* data are represented by six-pointed stars and infrared photometry from this study by open triangles. Other infrared photometry was taken from Vrba et al. (1976a, *five-pointed stars*), Taylor & Storey (1984, *circles with crosses*), Wilking et al. (1986, *slanted open squares*), and Price (1968, *open cross*). Optical photometry was taken from the Guide Star Catalog (*solid squares*), the SAO catalog (*open square*), Marraco & Rydgren (1981, *crosses*), and Vrba & Rydgren (1984, *open circles*). Fig. 3*a* presents SEDs for 7 Class I or flat-spectrum YSOs. Fig. 3*b* presents SEDs for 7 Class II objects. Fig. 3*c* shows SEDs for 11 Class III objects; the majority of these are believed to be field stars.

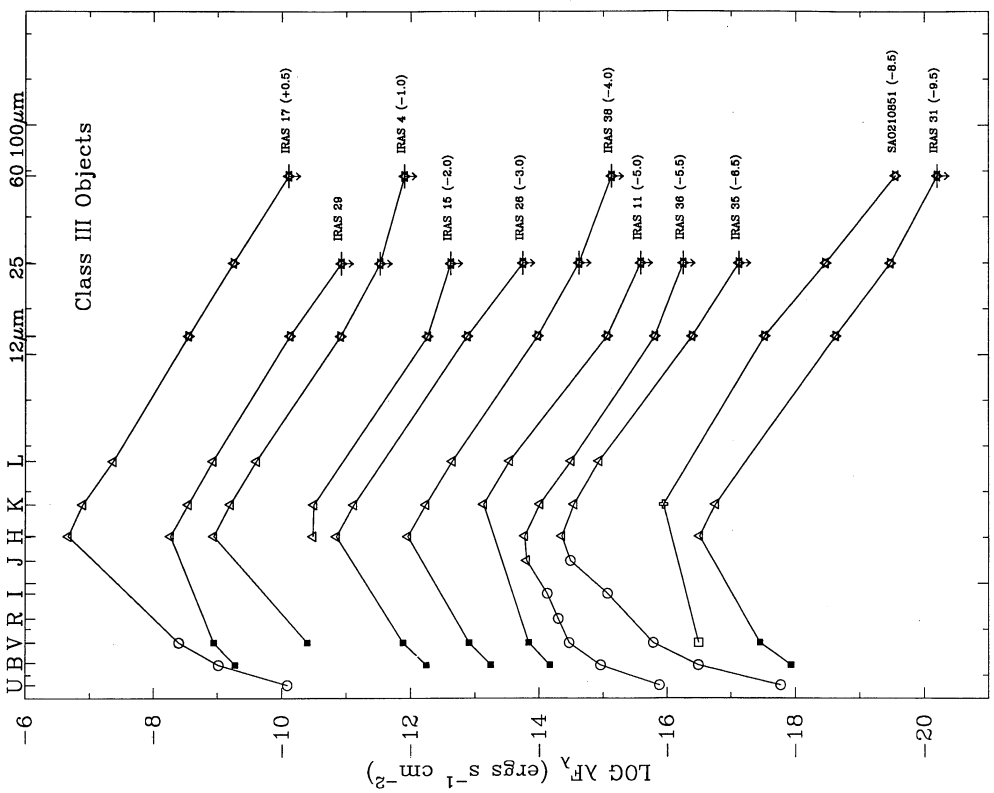

FIG. 3*c*

$A_v > 25$ mag), less massive (20 vs. 550 $M_\odot$), and has a lower peak visual extinction ($A_v = 45$ vs. 100 mag). Confusion in the *IRAS* data for the core of the R Cr A cloud is certainly prevalent due to extended emission from the stars R Cr A and TY Cr A and could mask the presence of lower luminosity sources. However, the overall lower extinctions in the Cr A cloud imply the *IRAS* data should be more complete than that in ρ Oph. This is confirmed by a plot of the number of all *IRAS* 12 μm sources versus their flux densities which indicates a much *higher* degree of completeness in the *IRAS* data for Cr A relative to ρ Oph.

The fact that there are fewer YSOs in Cr A relative to ρ Oph is also well documented at other wavelengths, using techniques which are not affected by source confusion. Objective prism surveys have produced only 17 Hα sources in the Cr A cloud while 65 are found in ρ Oph (Wilking, Schwartz, & Blackwell 1987). Near-infrared surveys of R Cr A have produced only 25 sources with a measured excess at 3.4 μm expected for YSOs with circumstellar disks (i.e., sources with $(K-L)/(H-K) > 0.70$ and $(K-L) > 0.4$, Jones & Hyland 1980). Forty-seven such objects have been identified in ρ Oph. Deep infrared imaging of the R Cr A core with an array camera to a detectable limit of $K = 17$ mag has been performed and a preliminary analysis rules out a large population of previously undetected low-luminosity YSOs (Rayner, McCaughrean, & Wilking 1992, unpublished observations). One could argue that many of the low-mass stars in Cr A are not seen because they have evolved into weak-emission objects with little or no infrared excess. However, analysis of X-ray observations of a 1.6 deg^2 area centered on S Cr A revealed only three potential weak-emission objects (Walter 1986).

The lower number of association members in Cr A is most likely attributed to the overall lower mass of both high-density and low-density molecular gas in the complex. We can compare directly three sets of mass estimates obtained from molecular-line observations made of the Cr A and ρ Oph clouds, each set obtained with the same telescope and spatial resolution. Low-resolution ^{12}CO surveys of both clouds, sensitive to the low-density component of molecular gas, have revealed a factor of 10 lower mass in the Cr A complex (3×10^4 $M_\odot$) relative to ρ Oph (3×10^5 $M_\odot$, Dame et al. 1987). A lower mass is also suggested from ^{13}CO data; Loren (1989) has estimated about 1450 $M_\odot$ for the L1688 cloud of the ρ Oph complex (the area considered by the *IRAS* study of Wilking et al. 1989) while a reexamination of the ^{13}CO column density maps in the R Cr A cloud (Loren 1979, Fig. 13) yields about 650 $M_\odot$. Similar differences in mass are clearly evident when comparing the amounts of high-density molecular gas; mapping of H_2CO emission from these clouds by Loren, Sandqvist, & Wootten (1983) has delineated gas with spatial densities in the range of 10^4–10^6 cm^{-3}. They have found the core mass in R Cr A to be only 19 $M_\odot$ compared to a total of 160 $M_\odot$ in ρ Oph. Complete mapping of the R Cr A cloud in a high-density tracer is needed to confirm the apparent scarcity of high-density gas.

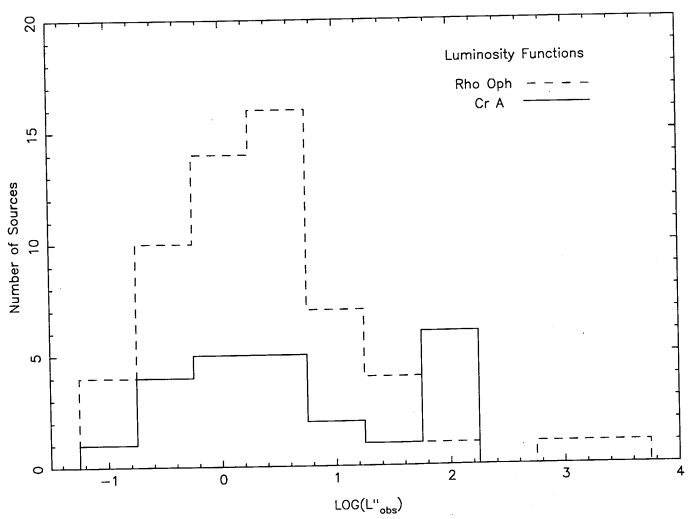

FIG. 4.—Luminosity functions for YSO populations in the ρ Ophiuchi cloud (*dashed lines*) and the Corona Australis complex (*solid lines*).

In summary, there is roughly a factor of 3 fewer YSOs in the Cr A cloud compared to the ρ Oph cloud. This ratio is firmly established by two surveys (*IRAS* and objective prism surveys) which have completely sampled these clouds. This ratio is roughly consistent with ratio of cloud masses derived from ^{13}CO observations over regions where YSOs have been studied. Therefore, given their similar ages, the star-formation efficiency in Cr A has been similar to that in the ρ Oph cloud. We expect that the final product of star formation in the R Cr A cloud will be a poor cluster or loose association of young stars. We note that the ratio of high-density molecular gas in Cr A compared to ρ Oph is currently much lower ($\sim$1/8.5) than the ratio of YSOs. If more comprehensive molecular-line observations reveal little additional high-density gas in Cr A, then star formation in the Cr A cloud could be regarded as *more* efficient than that in ρ Oph relative to their masses of high-density gas.

4.2. *Different Mass Functions?*

Differences between the two embedded populations are also evident when comparing the distributions of their YSO luminosities. This is demonstrated in Figure 4 where we plot the luminosity functions for Cr A and ρ Oph association members. Relative to the ρ Oph cloud, Cr A has fewer low-luminosity objects compared to the numbers of intermediate luminosity stars. For example, there are seven stars in both clouds with $L > 18$ $L_\odot$ but only 12 in the 0.56–18 $L_\odot$ range in Cr A compared to 37 in ρ Oph. This difference would become greater if one corrected for the fact that the *IRAS* data in ρ Oph are more incomplete at the lower luminosities due to the higher visual extinctions. We estimate that *IRAS* co-added survey data in Cr A completely sample both Class I and Class II sources down to 1 $L_\odot$; the ρ Oph data is complete down to 1 $L_\odot$ for Class I objects but becomes incomplete for Class II sources below 5 $L_\odot$. Hence, one is inclined to say either that the formation of low-mass stars has been inhibited in the Cr A cloud or the formation of intermediate mass stars has been enhanced.

As discussed in the previous section, the apparent deficiency of low-luminosity objects in Cr A relative to ρ Oph can be explained by the overall lower mass in the molecular complex. In fact, if one scales the number of Cr A sources in each luminosity bin up by a factor of 3, which is consistent with the mass difference between the two clouds, the luminosity functions are virtually indistinguishable from 0.06–56 $L_\odot$. The key to the difference in the luminosity functions appears to be the high number of objects (6) in Cr A with $L \sim 100$ $L_\odot$. Therefore, one is left with the possibilities that either the Cr A cloud has been

more efficient in the formation of intermediate luminosity objects relative to ρ Oph or that we have overestimated the number of intermediate luminosity stars associated with the Cr A cloud. It has been suggested that the double B8 star system, SAO 210815 and SAO 210816, did not actually form in the cloud but that they are field stars passing by the cloud (Marraco & Rydgren 1981). This conjecture is based on the fact that the stars are virtually unreddened and not associated with any high density or high column density gas unlike the other intermediate luminosity stars R Cr A, TY Cr A, and HD 176386 (Marraco & Rydgren 1981; Loren 1979). A similar argument could be forwarded for the B9.5 star SAO 210888 which lies in a gas-free area east of the cloud core. If we were to reduce the number of intermediate luminosity stars to three, then it is difficult to argue for a statistically significant excess of these stars relative to the number of lower luminosity objects.

5. SUMMARY

We have analyzed *IRAS* co-added survey data, Pointed Observations, and the PSC over a 57 pc^2 area of the Corona Australis dark cloud complex. By synthesizing these data with optical through mid-infrared wavelength data, we have investigated the number, distribution, evolutionary states, and bolometric luminosities of YSOs in the Cr A cloud complex. The major results are as follows:

1. The ratio of $S_\nu(25\ \mu\text{m})/S_\nu(12\ \mu\text{m}) = 0.8$ provides a good demarcation between association members and field stars. The majority of *IRAS* sources (64) have ratios less than 0.8 and are generally distributed uniformly across the complex; most of these sources are believed to be associated with field stars. There is a slight enhancement of these sources near the R Cr A cloud, but they avoid regions of high column density. All of the 15 sources with ratios greater than 0.8 appear to be young stellar objects, concentrated toward either the R Cr A cloud or Rossano Cloud B.

2. Spectral energy distributions and bolometric luminosities have been determined for 24 YSOs. Seven YSOs display Class I SEDs, four have flat SEDs, and eight have Class II SEDs. Five objects are early-type stars and display Class IIID SEDs. The roughly equal numbers of Class I and Class II objects is similar to that observed for the ρ Oph cluster. Also similar to ρ Oph is the possible segregation of source luminosities by SED class, with eight of nine sources with $L > 1.8\ L_\odot$ exhibiting either Class I or flat SEDs.

3. We have identified an extreme Class I source, IRAS 32, which has no detectable 12 μm emission and is associated with an extended near-infrared nebula. This source resembles other heavily obscured YSOs such as IRAS 16293−2422 and B335.

4. There are fewer YSOs observed in Cr A relative to the ρ Oph cloud. The lower number of YSOs is in rough proportion to the ratios of both low-density and high-density molecular gas between the two clouds. Since the duration of star formation in Cr A and ρ Oph has been similar (a few million yr), we conclude that the star formation efficiency in the Cr A cloud has been roughly the same as in ρ Oph.

5. The luminosity function of the Cr A cloud is unique as six of the 24 YSOs are intermediate-luminosity stars ($\sim 100\ L_\odot$) with spectral types ranging from B8 to A5. Either the cloud has formed intermediate-mass stars more efficiently than lower mass objects compared to other dark clouds, or some of these intermediate-mass objects are field stars which happen to be passing close to the cloud.

We would like to thank the many people who assisted with the collection and analysis of the data presented here. The folks at IPAC, particularly Gene Kopan, Greg Lairmore, and Deborah Levine, were extremely helpful and patient with our numerous requests for *IRAS* data. John Scalo generously provided us with the mosaic of BIGMAP images of Cr A which we use in Figure 1. We are grateful to Darren Depoy, Mark Shure, and Mike Ressler for their assistance with the acquisition and reduction of infrared array camera data from CTIO and the IRTF. We thank Joyce Watson and Doug Mink for their invaluable assistance in using SIMBAD and the Guide Star Catalog to identify *IRAS* sources. This research has made use of the SIMBAD database operated at CDS, Strausbourg, France. T. P. G. acknowledges support from a National Research Council-NASA Ames Research Associateship and C. J. L. from NSF grant AST 8815753. B. W. would like to thank Jim Moran for his hospitality during a research leave at the Center for Astrophysics and acknowledge support under NASA's Astrophysics Data Program and a University of Missouri Weldon Springs Award.

REFERENCES

Adams, F. C., Lada, C. J., & Shu, F. H. 1987, ApJ, 312, 788
———. 1988, ApJ, 326, 865
Boulanger, F. 1989, in Physics and Chemistry of Interstellar Molecules, ed. G. Winnewisser & J. T. Armstrong (Berlin: Springer), 30
Cruz-Gonzales, I., McBreen, B., & Fazio, G. G. 1984, ApJ, 279, 679
Dame, T. M., et al. 1987, ApJ, 322, 706
Elias, J. H., Frogel, J. A., Hyland, A. R., & Jones, T. J. 1983, AJ, 88, 1027
Elias, J. H., Frogel, J. A., Matthews, K., & Neugebauer, G. 1982, AJ, 87, 1029
Emerson, J. P. 1988, in Formation and Evolution of Low Mass Stars, ed. A. Dupree & M. T. V. T. Lago (Boston: Reidel), 1
Feast, M. W. 1963, MNRAS, 125, 367
Gauvin, L. S., & Strom, K. M. 1992, ApJ, 385, 217
Glass, I. S., & Penston, M. V. 1975, MNRAS, 172, 227 (GP)
Herbig, G. H. 1962, Adv. Astron. Astrophys., 1, 47
Iben, I., Jr. 1965, ApJ, 141, 993
IRAS Point Source Catalog 1985, Joint *IRAS* Science Working Group (Washington, DC: GPO)
Jones, T. J., & Hyland, A. R. 1980, MNRAS, 192, 359
Kenyon, S. J., Hartmann, L. W., Strom, K. M., & Strom, S. E. 1990, AJ, 99, 869
Knacke, R. F., Strom, K. M., Strom, S. E., & Young, E. T. 1973, ApJ, 179, 847
Lada, C. J. 1988, in Formation and Evolution of Low-Mass Stars, ed. A. Dupree & M. T. V. T. Lago (Dordrecht: Reidel), 93
Lada, C. J. 1991, in The Physics of Star Formation and Early Stellar Evolution, C. J. Lada & N. D. Kylafis (Dordrecht: Kluwer), 329
Lada, C. J., & Wilking, B. A. 1984, ApJ, 287, 610
Lasker, B. M., Sturch, C. R., McLean, B. J., Russell, J. L., Jenkner, H., & Shara, M. M. 1990, AJ, 99, 2019 (GSC)
Leene, A. 1986, A&A, 154, 295
Loren, R. B. 1979, ApJ, 227, 832
———. 1989, ApJ, 338, 902
Loren, R. B., Sandqvist, A., & Wootten, H. A. 1983, ApJ, 270, 620
Marraco, H. G., & Rydgren, A. E. 1981, AJ, 86, 62
Myers, P. M., Fuller, G. A., Mathieu, R. D., Beichmann, C. A., Benson, P. J., Schild, R. E., & Emerson, J. P. 1987, ApJ, 319, 340
Onlon, F. M., & Raimond, E. 1986, A&AS, 65, 607
Penny, A. J. 1979, MNRAS, 187, 829
Price, S. D. 1968, AJ, 73, 431
Prusti, T., Whittet, D. C. B., & Wesselius, P. R. 1992, MNRAS, in press
Rossano, G. S. 1978, AJ, 83, 234
Taylor, K. N. R., & Storey, J. W. V. 1984, MNRAS, 209, 5P (TS)
Tapia, S., & Whelan, J. 1975, ApJ, 200, 98
Vrba, F. J., Coyne, G. V., & Tapia, S. 1984, ApJ, 243, 489 (VCT)
Vrba, F. J., & Rydgren, A. E. 1984, ApJ, 283, 123
Vrba, F. J., Strom, S. E., & Strom, K. M. 1976a, AJ, 81, 317 (VSS)

Vrba, F. J., Strom, S. E., & Strom, K. M. 1976b, AJ, 81, 958 (VSSb)
Walter, F. M. 1986, ApJ, 306, 573
Wilking, B. A., Harvey, P. M., Joy, M., Hyland, A. R., & Jones, T. J. 1985, ApJ, 293, 165
Wilking, B. A., & Lada, C. J. 1983, ApJ, 274, 698
Wilking, B. A., Lada, C. J., & Young, E. T. 1989, ApJ, 340, 823
Wilking, B. A., Schwartz, R. D., & Blackwell, J. H. 1987, AJ, 94, 106
Wilking, B. A., Taylor, K. N. R., & Storey, J. W. V. 1986, AJ, 92, 103
Yorke, H. W. 1980, A&A, 85, 215